

On the Possibility of the Existence of Wormholes in Nature

Leonel Bixano* and Tonatiuh Matos†

*Departamento de Física, Centro de Investigación y de Estudios Avanzados del IPN,
Av. I.P.N. 2508, San Pedro Zacatenco, México 07360, CDMX.*

(Dated: June 12, 2025)

So far, many exotic predictions of Einstein's equations have been corroborated, with one exception: wormholes (WHs). In this work, we analyze an exact solution to the Einstein-Maxwell-Dilaton or Phantom equations representing rotating WHs. We introduce a ring singularity that, like other solutions, satisfies Wormhole Cosmic Censorship, i.e., the singularity is causally disconnected. We show that this WH is traversable through the poles, where tidal forces and the magnetic field are reasonably small. We satisfy the energy conditions for the dilaton-like solution. We argue that if dilaton-like interactions can exist in nature, for example, if extra dimensions exist as in superstring theory, WHs are a natural realistic prediction of Einstein's equations, and we should be able to observe them somehow, probably as black hole mimics. We give some examples of realistic WHs that could be observed in nature.

I. INTRODUCTION

Since Einstein's equations (EEq) were formulated in 1916 [1], their predictions have been stunning. Einstein himself predicted that his equations implied the existence of gravitational fluctuations, gravitational waves [2], but these are so small that, according to him, they are impossible to see or detect. Today, we have detected them hundreds of times [3], giving rise to a new era of astronomy where we detect astrophysical objects using gravitational waves instead of photons. In the same year, Karl Schwarzschild found the first exact, spherically symmetric solution to EEq [4]. Later, it was discovered that Schwarzschild's solution implies the existence of small, compact objects where light cannot escape [5]. Therefore, these objects were called black holes. At that time it was believed that the existence of these objects was impossible and that there must be a mechanism to prevent their existence. Today, we have at least two photographs of these objects [6] and hundreds of detections of collisions of these objects using gravitational waves [3]. One of the most interesting predictions of the EEq is the expansion of the universe. Even Einstein refused to accept it. He famously added the cosmological constant to his equations to prevent expansion [7], but without success. Today, we not only know that the universe is expanding [8], but that it is accelerating [9], something Einstein's equations cannot predict. And so on. To date, we are unaware of any important physical predictions of Einstein's equations that cannot be observed or detected, with the exception of wormholes (WH) [10]. The high level of prediction of the EEq is astonishing, and many of them are surprising.

In this work, we analyze exact solutions of the EEq equipped with an electromagnetic field and a scalar field that can be dilaton-type (i.e., real and coupled to the electromagnetic field) or ghost-type (i.e., with a negative

kinetic term in the Lagrangian). We show them using two parameters: the parameter ϵ_0 , which takes the value 1 for the dilaton field and -1 for the ghost field, and the parameter α_0 to distinguish them from different theories. In [11], different values for the parameter α_0 are used to derive solutions that correspond to examples of compact objects. The exact solutions are general for almost any value of these parameters, subject to a constraint equation. The solutions present a ring singularity encased by the throat. However, here we show, as in previous solutions, that the geodesics cannot touch it or that the geodesic will need infinite time to approach it. We call this phenomenon Wormhole Cosmic Censorship [12, 13], it has been observed in several exact WH solutions of the EEq [11, 14–17]. Furthermore, these solutions satisfy the energy conditions for $\epsilon_0 = 1$, and we provide the region where these solutions are traversable. Finally, we show different possibilities for the mass of these solutions where they can be realistic, basing the value of the free parameters on where they can lie. We find several possibilities and different types of compact objects that can be considered WH rather than compact objects, that is, objects in the cosmos where WHs mimic well the properties of the objects we observe. This raises the possibility that some cosmic objects could be WH rather than compact objects, provided that the dilaton interaction is possible. This interaction can exist in nature and is a necessity if extra dimensions exist.

In this work, we employ the Einstein-Maxwell-Dilaton (EMD) theory to derive a novel combination solution that are composed by two distinct solutions that have been previously investigated in [18] and [19]. In this instance, we start with a Lagrangian expressed in the International System of Units (SI), which has energy density units

$$\mathfrak{L} = \sqrt{-g} \left(-\frac{c^4}{8\pi G} R + \frac{c^4}{8\pi G} 2\epsilon_0 (\nabla\phi)^2 + \frac{1}{\mu_0} e^{-2\alpha_0\phi} F^2 \right), \quad (1)$$

* Contact author: leonel.delacruz@cinvestav.mx

† Contact author: tonatiuh.matos@cinvestav.mx

where c is the speed of light, G is the gravitational constant, and μ_0 the vacuum permeability. ϕ denotes the scalar field and is characterised as dimensionless. The parameter α_0 specifies the theoretical framework employed and has the potential to adopt the values

$$\alpha_0^2 = \begin{cases} 1/12 & \Rightarrow \mathcal{L} \text{ corresponds to} \\ & \text{Entangled Relativity lagrangian} \\ 3 & \Rightarrow \mathcal{L} \text{ corresponds to} \\ & \text{Kaluza-Klein lagrangian} \\ 1 & \Rightarrow \mathcal{L} \text{ corresponds to Low-Energy} \\ & \text{Super Strings lagrangian} \\ 0 & \Rightarrow \mathcal{L} \text{ corresponds to} \\ & \text{Eintein-Maxwell lagrangian} \end{cases} \quad (2)$$

and ϵ_0 take only two values, 1 if ϕ is a dilatonic scalar field and -1 if it is a phantom scalar field. $F_{\mu\nu}$ is the Faraday tensor that has units of teslas and R is the Ricci scalar with length⁻² units.

Defining an important constant that gives the correct units to the 4-potential

$$\sigma_0 \equiv \frac{8\pi G}{\mu_0 c^4} \quad \text{implies} \quad \frac{1}{\sqrt{\sigma_0}} \approx 2.46 \times 10^{18} [\text{Meters} * \text{Teslas}], \quad (3)$$

The corresponding field equations of the Lagrangian (1) are:

$$\nabla_\mu (e^{-2\alpha_0\phi} F^{\mu\nu}) = 0, \quad (4a)$$

$$\epsilon_0 \nabla^2 \phi + \frac{\alpha_0}{2} \sigma_0 (e^{-2\alpha_0\phi} F^2) = 0, \quad (4b)$$

$$R_{\mu\nu} = 2\epsilon_0 \nabla_\mu \phi \nabla_\nu \phi + 2\sigma_0 e^{-2\alpha_0\phi} \left(F_{\mu\sigma} F_\nu^\sigma - \frac{1}{4} g_{\mu\nu} F^2 \right), \quad (4c)$$

where $\nabla^2 = \nabla^\mu \nabla_\mu$. The above equations are, in general, very difficult to solve. There is a way to solve them for the axisymmetric stationary case given in [11].

II. PREVIOUS SOLUTIONS.

Cylindrical coordinates (ρ, z) will serve as a fundamental tool for performing physical analyses. However, for mathematical processes, Lewis-Papapetrou coordinates (x, y) are more advantageous; the relationship between them is

$$\rho^2 = L^2(x^2 + 1)(1 - y^2), \quad z = Lxy, \quad (5)$$

where $\rho \in [0, \infty)$, $\{z, x\} \in \mathbb{R}$, and $y \in [-1, 1]$.

The variables $\{\rho, z, L\}$ have units of length and L is related to the size of the WH throat, as we will see later. The variables $\{x, y\}$ are dimensionless.

Another important set of coordinates are the Boyer-Lindquist coordinates (r, θ) , which are advantageous for investigating physical phenomena. These are related to the coordinates mentioned above as

$$Lx = r - l_1, \quad y = \cos \theta, \quad (6)$$

for this case, $r \in (-\infty, -l_1] \cup [l_1, \infty)$. $\theta \in [0, \pi]$, and the variable $l_1 = X_i/2$, where X_i is the Schwarzschild radius has units of length. Furthermore, there exists a significant relationship between variables L and l_1 , which is expressed as the equation

$$L^2 + l_1^2 = l_0^2 \equiv a^2 + Q_L^2 + H_L^2 \quad (7)$$

where a is the rotational moment per unit mass, Q_L and H_L are the electric and magnetic charges, respectively. To express the parameters in SI, we must consider the expressions

$$l_1 = \frac{MG}{c^2} \quad [=] \quad \text{Length}, \quad (8a)$$

$$J_k \equiv \frac{2GJ}{c^3} \quad [=] \quad \text{Length}^2, \quad (8b)$$

$$a \equiv \frac{J_k}{2l_1} \quad [=] \quad \text{Length}, \quad (8c)$$

$$Q_L^2 \equiv \frac{G}{c^4} \frac{Q^2}{\epsilon_0} \quad [=] \quad \text{Length}^2, \quad (8d)$$

$$H_L^2 \equiv \frac{G}{c^4} \frac{H^2}{\mu_0} \quad [=] \quad \text{Length}^2, \quad (8e)$$

$$l_0^2 \equiv a^2 + Q_L^2 + H_L^2 \quad [=] \quad \text{Length}^2, \quad (8f)$$

where J possesses units of angular momentum, M corresponds to units of mass, and $\{Q, H\}$ are characterized by the units of electric charge and magnetic charge, respectively.

We start from a space-time with two commutative symmetries, that is, in this space-time there are two Killing vectors $\partial_\phi, \partial_t$, which allow us to write the metric in cylindrical coordinates (ρ, z) as

$$ds^2 = -f \left\{ d(ct) - \frac{\omega}{L} d(L\varphi) \right\}^2 + f^{-1} \left\{ e^{2k} (d\rho^2 + dz^2) + \frac{\rho^2}{L^2} d(L\varphi)^2 \right\}, \quad (9)$$

where $\{f, \omega, \kappa\}$ are the metric functions that depend on the coordinates (ρ, z) , $\{f, \kappa\}$ are dimensionless, and ω has units of length. If we want the representation of the metric in (x, y) , the expression (9) takes the form:

$$ds^2 = -f \left(d(ct) - \frac{\omega}{L} d(L\varphi) \right)^2 + f^{-1} \left((x^2 + 1)(1 - y^2) d(L\varphi)^2 + L^2(x^2 + y^2) e^{2k} \left\{ \frac{dx^2}{x^2 + 1} + \frac{dy^2}{1 - y^2} \right\} \right), \quad (10)$$

Using the symmetries of space-times, the electromagnetic 4-Potential is reduced to

$$A_\mu = \left[A_t(\rho, z), 0, 0, A_\varphi(\rho, z) \right]. \quad (11)$$

Next, we solve the equations (4) using the method proposed in [14]. To do this, the method defines the potentials.

$$\tilde{D}\chi = \sigma_0 \frac{2f\kappa^2}{\rho} L \left(\frac{\omega}{L} DA_t + DA_\varphi \right), \quad (12a)$$

$$\tilde{D}\epsilon = \frac{f^2}{\rho} D\omega + \psi \tilde{D}\chi, \quad (12b)$$

$$\psi = 2A_t, \quad (12c)$$

where the differential operators D, \tilde{D} are

$$D = \begin{bmatrix} \partial_\rho \\ \partial_z \end{bmatrix}, \quad \tilde{D} = \begin{bmatrix} \partial_z \\ -\partial_\rho \end{bmatrix}. \quad (13)$$

To simplify the notation we define the vector potential Y^A

$$(Y^A) = \begin{bmatrix} f \\ \epsilon \\ \psi \\ \chi \\ \kappa \end{bmatrix} [=] \begin{bmatrix} \text{dimensionless} \\ \text{dimensionless} \\ \text{length} * \text{tesla} \\ (\text{length} * \text{tesla})^{-1} \\ \text{dimensionless} \end{bmatrix}, \quad (14)$$

which are respectively the gravitational, rotational, electric, magnetic and scalar potentials.

Substituting the metric (9), the 4-potential (11), and the definitions (12) into the field equations (4), these reduce to

Klein-Gordon equation

$$D(\rho D\kappa) - \frac{\rho}{\kappa} D\kappa^2 + \frac{\rho\kappa^3\alpha_0^2}{4f\epsilon_0}\sigma_0 \left(D\psi^2 - \frac{1}{\kappa^4(\sigma_0)^2} D\chi^2 \right) = 0, \quad (15a)$$

Maxwell equations

$$D(\rho D\psi) + \rho D\psi \left(\frac{2D\kappa}{\kappa} - \frac{Df}{f} \right) - \frac{\rho}{f\kappa^2\sigma_0} (D\epsilon - \psi D\chi) D\chi = 0, \quad (15b)$$

$$D(\rho D\chi) - \rho D\chi \left(\frac{2D\kappa}{\kappa} + \frac{Df}{f} \right) + \frac{\rho\kappa^2}{f}\sigma_0 (D\epsilon - \psi D\chi) D\psi = 0, \quad (15c)$$

Einstein equations

$$D(\rho Df) + \frac{\rho}{f} ((D\epsilon - \psi D\chi)^2 - Df^2) - \frac{\rho\kappa^2}{2}\sigma_0 \left(D\psi^2 + \frac{1}{\kappa^4(\sigma_0)^2} D\chi^2 \right) = 0, \quad (15d)$$

$$D(\rho(D\epsilon - \psi D\chi)) - \frac{2\rho}{f}(D\epsilon - \psi D\chi)Df = 0. \quad (15e)$$

The next step in the method is to use the ansatz $Y^A = Y^A(\lambda)$, where $\lambda = \lambda(x, y)$, satisfies Laplace's equation

$$\partial_x \{ (x^2 + 1) \partial_x \lambda \} + \partial_y \{ (1 - y^2) \partial_y \lambda \} = 0. \quad (16)$$

With this ansatz, the field equation is considerably reduced and can be solved in some way, see [15] and [14]. Using the method described in the mentioned papers allows the derivation of the second family of solutions.

$$f = f_0, \quad \kappa = \kappa_0 e^\lambda, \quad \psi = \frac{\sqrt{f_0}}{\sqrt{\sigma_0 \kappa_0}} e^{-\lambda} + \psi_0, \\ \chi = \sqrt{\sigma_0} \sqrt{f_0 \kappa_0} e^\lambda + \chi_0, \quad \epsilon = b_0, \quad (17)$$

where $\{f_0, \psi_0, \chi_0, \kappa_0, b_0\}$ are integration constants.

From the definitions of potentials (12), we can integrate the components of the metric [20]

$$\begin{bmatrix} \partial_x \\ \partial_y \end{bmatrix} \omega = \frac{L}{f^2} (\epsilon, \lambda - \psi \chi, \lambda) \begin{bmatrix} (1 - y^2) \partial_y \\ -(x^2 + 1) \partial_x \end{bmatrix} \lambda, \quad (18a)$$

$$\begin{bmatrix} \partial_x \\ \partial_y \end{bmatrix} A_\varphi = \frac{1}{2\sigma_0 f \kappa^2} (\chi, \lambda) \begin{bmatrix} (1 - y^2) \partial_y \\ -(x^2 + 1) \partial_x \end{bmatrix} \lambda - \frac{\omega}{2L} (\psi, \lambda) \begin{bmatrix} \partial_x \\ \partial_y \end{bmatrix} \lambda, \quad (18b)$$

$$\partial_x k = k_0 \frac{1 - y^2}{x^2 + y^2} \left\{ -2y(x^2 + 1)(\partial_x \lambda)(\partial_y \lambda) + x[(x^2 + 1)(\partial_x \lambda)^2 - (1 - y^2)(\partial_y \lambda)^2] \right\}, \quad (18c)$$

$$\partial_y k = k_0 \frac{x^2 + 1}{x^2 + y^2} \left\{ 2x(1 - y^2)(\partial_x \lambda)(\partial_y \lambda) + y[(x^2 + 1)(\partial_x \lambda)^2 - (1 - y^2)(\partial_y \lambda)^2] \right\}, \quad (18d)$$

where k_0 is an integration constant, $F, \lambda = \partial F / \partial \lambda$, for any function F .

Two solutions taken from [14], of equation (16), are

$$\lambda_5 = \lambda_0 \frac{x}{(x^2 + y^2)} + m_0, \quad (19a)$$

$$\lambda_6 = \lambda_0 \frac{y}{(x^2 + y^2)} + m_0, \quad (19b)$$

where λ_0 and m_0 are integration constants. For our propose $m_0 = 0$.

This solutions are already analyzed in [19] for λ_5 and in [11] for λ_6 .

The functions metric and the 4-potential to λ_5 are

$$f = f_0 = 1, \quad (20a)$$

$$\omega = -L \frac{\lambda_0}{f_0} \left(\frac{y(x^2 + 1)}{x^2 + y^2} \right), \quad (20b)$$

$$A_\varphi = -\frac{\sqrt{f_0}}{2\kappa_0\sqrt{\sigma_0}} \frac{\omega}{L} e^{-\lambda_5}, \quad (20c)$$

$$A_t = \frac{\sqrt{f_0}}{2\kappa_0\sqrt{\sigma_0}} e^{-\lambda_5}, \quad (20d)$$

$$k_{\lambda_5} = -k_0\lambda_0^2 \frac{(1-y^2)}{4(x^2+y^2)^4} \left(-8x^2y^2(x^2+1) + [x^2+y^2]^2 [(1-y^2) + 2(x^2+y^2)] \right). \quad (20e)$$

On the other hand, for λ_6 is

$$f = f_0 = 1, \quad (21a)$$

$$\omega = \frac{L\lambda_0}{f_0} \frac{x(1-y^2)}{x^2+y^2}, \quad (21b)$$

$$A_\varphi = -\frac{\sqrt{f_0}}{2\kappa_0\sqrt{\sigma_0}} \frac{\omega}{L} e^{-\lambda_6}, \quad (21c)$$

$$A_t = \frac{\sqrt{f_0}}{2\kappa_0\sqrt{\sigma_0}} e^{-\lambda_6}. \quad (21d)$$

$$k_{\lambda_6} = -k_0\lambda_0^2 \frac{(1-y^2)}{4(x^2+y^2)^4} \left(8x^2y^2(x^2+1) - [x^2+y^2]^2(1-y^2) \right). \quad (21e)$$

Both regular solutions represent a rotating electromagnetic WH with no gravitational potential.

III. NEW COMBINATION SOLUTION

Using the linearity of the equation (16), we can obtain a new solution by combining two or more of these. Two interesting solutions are (21) and (20), which represent a magnetic monopole and a magnetic dipole respectively. The combined solution λ_c reads

$$\lambda_c = \frac{\lambda_0 y + \tau_0 x}{(x^2 + y^2)}. \quad (22)$$

The corresponding dilatonic scalar field takes the form

$$\phi(x, y) = -\frac{\lambda_c}{\alpha_0}. \quad (23)$$

whose asymptotic behavior is

$$\lim_{x \rightarrow \pm\infty} \phi(x, y) = 0,$$

which implies that the scalar field remains bounded.

Thus, the metric functions of the solution (22) obtained by the equations (18) are

$$f = f_0 = 1, \quad (24a)$$

$$\omega = \frac{L}{f_0} \left(\frac{\lambda_0 x(1-y^2) - \tau_0 y(x^2+1)}{x^2+y^2} \right), \quad (24b)$$

$$A_\varphi = \frac{\sqrt{f_0}}{2\kappa_0\sqrt{\sigma_0}} \left(A_3 - \frac{\omega}{L} e^{-\lambda_c} \right), \quad (24c)$$

$$A_t = \frac{\sqrt{f_0}}{2\kappa_0\sqrt{\sigma_0}} \left(e^{-\lambda_c} - 1 \right) \quad (24d)$$

$$k_c = k_{\lambda_5} + k_{\lambda_6} \quad (24e)$$

$$-k_0 \frac{8xy(1-y^2)(x^2+1)(x^2-y^2)\lambda_0\tau_0}{4(x^2+y^2)^4}, \quad (24f)$$

where A_3 is a constant to ensure that A_φ remains finite as x approaches infinity.

Note that the asymptotic behavior of the metric functions is as follows

$$\lim_{x \rightarrow \pm\infty} \omega(x, y) = -\tau_0 L y, \quad (25a)$$

$$\omega(0, y) = -\frac{\tau_0 L}{y}, \quad (25b)$$

$$\omega(x, 0) = \frac{L\lambda_0}{x}, \quad (25c)$$

$$\omega(x, 1) = -L\tau_0, \quad (25d)$$

$$\text{For } x \gg 1 \text{ we have } k_c \approx -k_0\tau_0^2 \frac{(1-y^2)}{2x^2}, \quad (26a)$$

$$k_c(0, y) = \frac{k_0(1-y^2)}{4y^4} \{ \lambda_0^2(1-y^2) - \tau_0^2(1+y^2) \}, \quad (26b)$$

$$k_c(x, 0) = k_0 \frac{(\lambda_0^2 - \tau_0^2(2x^2+1))}{4x^4}, \quad (26c)$$

$$k_c(x, 1) = 0. \quad (26d)$$

In the same way as in [19], and [18], we substitute the solution (24) associated with λ_c , and the scalar field (23), in (4) to obtain a constraint on the free parameters of the solution, this is

$$\alpha_0^2(4k_0 + 1) - 4\epsilon_0 = 0. \quad (27)$$

In Table I we present the allowed values for the k_0 parameter, (see also [18] and [19]).

IV. RING SINGULARITY AND ASYMPTOTICALLY FLATNESS

To study the metric singularities of space-time, we can use two important scalars, the Ricci scalar $R = g^{\alpha\beta} R_{\alpha\beta} = g^{\alpha\beta} R^\sigma_{\alpha\sigma\beta}$ and the Kretschmann scalar $KN = R^{\mu\nu\alpha\beta} R_{\mu\nu\alpha\beta}$. The invariants R and KN associated to (λ_c) are

$$R = \frac{(4k_0 + 1)e^{-2k_c}}{2L^2(x^2 + y^2)^4} \left\{ \lambda_0^2 \left(y^2(1 - y^2) + x^2(3y^2 + 1) \right) + \tau_0^2 \left(y^2 + x^2(x^2 - 3y^2 + 1) \right) + 4\lambda_0\tau_0xy(x^2 - y^2) \right\}, \quad (28a)$$

$$KN = \frac{F_5(x, y)}{8L^4(x^2 + y^2)^{12}} e^{-4k(x, y)}, \quad (28b)$$

where, $F_5(x, y)$ is a polynomial of degree less than $(x^2 + y^2)^{12}$.

Using (26a), the asymptotic behavior of (28a) reads

$$\lim_{x \rightarrow \pm\infty} e^{k_c} = 1,$$

for any sign of k_0 . Therefore

$$\text{for } x \gg 1 \text{ we have } R \approx (4k_0 + 1) \frac{\tau_0^2}{2L^2x^4}, \quad (29)$$

Consequently, R tends to zero for any sign of $(4k_0 + 1)$, in other words, spacetime is asymptotically flat for both the dilatonic and ghost scalar fields. On the other hand, (28b) indicates the existence of a ring singularity at $x = y = 0$, which corresponds to $r = l_1$ and $\theta = \pi/2$ in Lewis-Papapetrou coordinates or $\rho = L$ and $z = 0$ in cylindrical coordinates. We will observe later that this ring singularity is causally disconnected.

V. NULL ENERGY CONDITION

The Null Energy Condition (NEC) is determinate by the following inequality

$$T_{\mu\nu} l^\mu l^\nu \geq 0,$$

where l^μ is the null vector, i.e., satisfies $l^\mu l_\mu = 0$, and $T_{\mu\nu}$ is the energy-momentum tensor. To study the NEC, it is necessary to define the comoving reference system \mathbb{O} , which physically corresponds to a frame fixed to the compact object. For this purpose, we will use a tetrad that transforms the basis of the tangent space corresponding to the coordinate system of \mathbb{O} . The matrix representation of the tetrad is

$$\mathbb{M}_{comoving}^T = \begin{bmatrix} 1/\sqrt{-g_{tt}} & 0 & 0 & 0 \\ 0 & 1/\sqrt{g_{xx}} & 0 & 0 \\ 0 & 0 & 1/\sqrt{g_{yy}} & 0 \\ \frac{-g_{\varphi t}/g_{tt}}{Det_{\varphi t}} & 0 & 0 & \frac{1}{Det_{\varphi t}} \end{bmatrix}. \quad (30)$$

TABLE I: Values of k_0

α_0^2	Dilatonic field ($\epsilon_0 = 1$)	Phantom field ($\epsilon_0 = -1$)
1/12	143	-145
1	3/4	-5/4
3	1/12	-7/12
4	0	-1/2
$n \geq 5$	$(4 - n)/4n$	$-(4 + n)/n$

where $Det_{\varphi t} = \sqrt{g_{\varphi\varphi} - (g_{\varphi t})^2/g_{tt}}$. Thus, the relationships between the basis vector in \mathbb{O} and the bases of the coordinate system are

$$\begin{bmatrix} \partial_0 \\ \partial_1 \\ \partial_2 \\ \partial_3 \end{bmatrix}^T = \mathbb{M}_{comoving}^T \begin{bmatrix} \partial_t \\ \partial_x \\ \partial_y \\ \partial_\varphi \end{bmatrix}^T. \quad (31)$$

We use the indices $a, b = 0, \dots, 3$ for \mathbb{O} and α, β, \dots for our coordinate system, so the Ricci tensor transforms as

$$R_{ab} = \mathbb{M}_{comoving} \cdot \{R_{\mu\nu}\} \cdot (\mathbb{M}_{comoving})^T.$$

We can fix the null vector as $l_a = e_0 + e_1$, with this the NEC in \mathbb{O} is

$$\begin{aligned} T_{ab} l^a l^b &= T_{00} + T_{11} = \varrho - P \\ &= \frac{c^4}{8\pi G} \left(R_{00} + R_{11} \right) \geq 0, \end{aligned} \quad (32)$$

where ϱ is the density and P the pressure.

For the second class of solutions (17), we find that the density satisfies the following condition

$$\begin{aligned} \frac{8\pi G}{c^4} \varrho = R_{00} &= \frac{e^{-2k}}{2L^4(x^2 + 1)(1 - y^2)(x^2 + y^2)} \\ &\left((1 - y^2)\omega_{,y}^2 + (x^2 + 1)\omega_{,x}^2 \right) \geq 0, \end{aligned} \quad (33)$$

Observe that there are only quadratic terms in (33), then for this second family of solutions $\varrho \geq 0$.

On the other hand, the expression for the pressure is

$$\begin{aligned} \frac{8\pi G}{c^4} P = R_{11} &= -\frac{e^{-2k}}{L^2(x^2 + y^2)} \left((1 - y^2)k_{,yy} \right. \\ &\left. + (x^2 + 1)k_{,xx} - 2yk_{,y} - \frac{\omega_{,x}^2}{2L^2(1 - y^2)} \right), \end{aligned} \quad (34)$$

for constant scalar field and rotation, $P = 0$.

By substituting metric functions of λ_c (24) the NEC is

$$\varrho - P = \frac{e^{-2k_c}}{2L^2(x^2 + y^2)^5} \left\{ 4\lambda_0\tau_0xy(x^2 - y^2)(x^2 + 2y^2 - 1 + 4k_0(x^2 + 1)) + 2\lambda_0^2(y^4(1 - y^2) + x^4(1 + (1 + 8k_0)y^2) + 2(4k_0 + y^2)x^2y^2) + \tau_0^2[(4k_0 + 1)(x^2 + 1)x^4 - 2x^2y^2(4k_0(x^2 + 1) + x^2 - 3) + (1 + 4k_0 + (4k_0 - 7)x^2)y^4] \right\}, \quad (35)$$

In the following we will evaluate the zero energy condition (35). Initially, it is imperative to obtain the expression that represents the extreme values of x and y , similarly, the intermediate regions corresponding to $x \approx y$. It is worth noting that $y \in [-1, 1]$ implies $y^{2n} \in [0, 1]$ appears in one case, $x \in (-\infty, \infty)$ implies $x^{2n} \in [0, \infty)$, then

$$\text{For } x \gg 1 \text{ implies } (\varrho - P) \approx \frac{(4k_0 + 1)\tau_0^2}{2L^2x^4}, \quad (36a)$$

$$\lim_{x \rightarrow 0} (\varrho - P) = \frac{e^{-2k_c(0,y)}}{2L^2y^6} \left\{ 2\lambda_0^2(1 - y^2) + \tau_0^2(4k_0 + 1) \right\}, \quad (36b)$$

$$\lim_{x \rightarrow y} (\varrho - P) = \frac{e^{-2k_c(y,y)}}{16L^2y^6} \left\{ 2\tau_0^2(1 - y^2) + \lambda_0^2(4k_0 + 1)(1 + y^2) \right\}, \quad (36c)$$

$$(\varrho - P)|_{y=0} = \frac{e^{-2k_c(x,0)}}{2L^2x^6} \left\{ 2\lambda_0^2 + \tau_0^2(4k_0 + 1)(x^2 + 1) \right\}, \quad (36d)$$

$$(\varrho - P)|_{y=1} = (4k_0 + 1) \frac{(2\lambda_0x + \tau_0\{x^2 - 1\})^2}{2L^2(x^2 + 1)^4}. \quad (36e)$$

Using the equation (36a), it is evident that in the asymptotic region ($x \gg 1$), the key term in determining whether the NEC holds is $(4k_0 + 1)$. This is because, when considering the limit where $x \rightarrow \infty$, $(\varrho - P)$ approaches 0^\pm , the outcome depends on whether $(4k_0 + 1) > 0$ or $(4k_0 + 1) < 0$. Specifically, whether the limit approaches zero from the positive region 0^+ or the negative region 0^- determines whether the NEC holds or not.

In the intermediate regions $x \approx y$, the equation (36c) shows that the key term is $(4k_0 + 1)$. This is because, given $y \in [-1, 1]$ and subsequently $y^{2n} \in [0, 1]$ implies $1 - y^2 > 0$, the exponential function is positive. We also know that $\lambda_0, \tau_0 \in \mathbb{R}$, so the only significant term determining whether the NEC holds is the second term on the right-hand side of the equation (36c). In short, the crucial term in the intermediate regions is, once again, $(4k_0 + 1)$.

Another critical region arises when considering $x \ll 1$. Examination of the right-hand side of the equation (36b) reveals that the only factor responsible for violating the

NEC is, once again, $(4k_0 + 1)$, since the first term remains invariably positive, the exponential function is positive, and $y^2 + 1 > 0$. The most critical points for analysis are the extremes, when the conditions $y = 0$ or $y = 1$ are met. From (36d) and (36e), it follows that all components constituting the aforementioned equalities are positive, with the exception of the $(4k_0 + 1)$ term. Therefore, for the entire region examined, we find that

$$\begin{aligned} \text{If } 4k_0 + 1 > 0 & \text{ implies } (\varrho - P) > 0, \\ \text{If } 4k_0 + 1 < 0 & \text{ implies } (\varrho - P) < 0. \end{aligned}$$

In summary, we have obtained the known result that

$$\begin{aligned} \text{Dilatonic Field} & \text{ implies } (\varrho - P) > 0, \\ \text{Phantom Field} & \text{ implies } (\varrho - P) < 0. \end{aligned}$$

VI. WORMHOLE GEOMETRY

To analyze WH geometry, the use of embedding diagrams is essential. Initially, the WH is embedded in a cylindrical plane using two different methods. These methods involve selecting a hypersurface with parameter $t = t_0$ and another variable kept constant, depending on the desired shape visualization. Setting $y = y_0$ yields a diagram illustrating the throat connecting two regions. Conversely, using $x = x_0$ yields the throat shape. Examples of this procedure, along with detailed explanations, can be found in [21] and [22].

In our case $f = 1$, then we take $t = t_0$ and $y = y_0$ in (10), we arrive to

$$ds^2 = L^2 \frac{(x^2 + y_0^2)e^{2k(x,y_0)}}{x^2 + 1} dx^2 + [L^2(x^2 + 1)(1 - y_0^2) - \omega(x, y_0)^2] d\varphi^2. \quad (37)$$

Fixing $t = t_0$ and $x = x_0$ in (10), we acquired

$$ds^2 = L^2 \frac{(x_0^2 + y^2)e^{2k(x_0,y)}}{1 - y^2} dy^2 + [L^2(x_0^2 + 1)(1 - y^2) - \omega(x_0, y)^2] d\varphi^2. \quad (38)$$

We will use a flat cylindrical space representation (x, y) , and consider a parameterization with respect to

x^i at constant $x^j \neq x^i$, where if $x^i = x$ implies $x^j = y_0$ or $x^i = y$ implies $x^j = x_0$

$$ds^2 = d\bar{\rho}^2 + dz^2 + \bar{\rho}^2 d\varphi^2$$

$$= \left\{ \left(\frac{d\bar{\rho}}{dx^i} \right)^2 + \left(\frac{dz}{dx^i} \right)^2 \right\} (dx^i)^2 + \bar{\rho}(x^i, (x_0)^j)^2 d\varphi^2, \quad (39)$$

where $\bar{\rho}$ is the corresponding radial variable in the coordinates of the cylindrical plane. It is possible to embed the hypersurface (37) or (38) in (39), that is, to equate the corresponding metric elements to derive differential equations, which will be solved numerically and subsequently visualized in a figure. The 2 differential equation systems that arise from the embedding, are

$$\bar{\rho}(x, y_0)^2 = L^2(x^2 + 1)(1 - y_0^2) - \omega(x, y_0)^2, \quad (40a)$$

$$\left(\frac{d\rho}{dx} \right)^2 + \left(\frac{dz}{dx} \right)^2 = L^2 \frac{(x^2 + y_0^2)}{x^2 + 1} e^{2k(x, y_0)}. \quad (40b)$$

$$\bar{\rho}(x_0, y)^2 = L^2(x_0^2 + 1)(1 - y^2) - \omega(x_0, y)^2, \quad (41a)$$

$$\left(\frac{d\rho}{dy} \right)^2 + \left(\frac{dz}{dy} \right)^2 = L^2 \frac{(x_0^2 + y^2)}{1 - y^2} e^{2k(x_0, y)}. \quad (41b)$$

Solving numerically and obtaining $\bar{\rho}(x), \bar{\rho}(y)$ and $z(x), z(y)$, we can graph $z(\bar{\rho})$ with the initial condition (see Figure 1).

Figure 1a illustrates several curves, each graphed in a different color, that represent the embedding hypersurface for different values according to $y_0 = \cos \theta_0$. These correspond to the numerical solution presented in (40). The black dashed line indicates the size of the WH as specified by $L = 1 \text{ Km}$, holding the condition $L < 2l_1$. It can be observed that, in the vicinity of the equatorial plane, the geometry assumes a flat configuration, while at the poles it resembles a cylindrical shape. To understand the three-dimensional shape, one can examine Figure 2, which illustrates the surface representation of each curve shown in the Figure 1a, now represented in three dimensions.

As illustrated in Figure 1b, the shape of the throat is represented by curves of different colors, each corresponding to discrete values of x_0 , a value that approaches L under the condition $x = 0$. Similarly, the figure demonstrates that the configuration becomes flat as we approach the point $x = 0$; this implies that, as the system approaches the ring singularity, the WH geometry tends to close. The figure illustrates a discontinuity in the curves, denoted by the $z = 0$ values, this is because the system of differential equations (41) is not defined at the point $y = 1$.

The last plot presented in Figure 1 shows the three-dimensional graphs corresponding to the surfaces of revolution generated by the curves in 1a, evaluated for various values of y_0 . It should be noted that not all curves are included to avoid overloading the illustration.

The radial coordinates determining the size of the WH are given by (40a). However, in this case, the throat size depends on the angular position, given by y . Consequently, the throat size of an axisymmetric WH has the minimum value at $\bar{\rho}(0, y_0)$ for each y_0 .

VII. TIDAL FORCES

Following the methodology proposed in [23] (see also [18], and [19]), the most appropriate reference frame for analyzing tidal forces is that of an astronaut $\hat{\mathcal{O}}$ attempting to cross the WH. For simplicity, in the astronaut's ref-

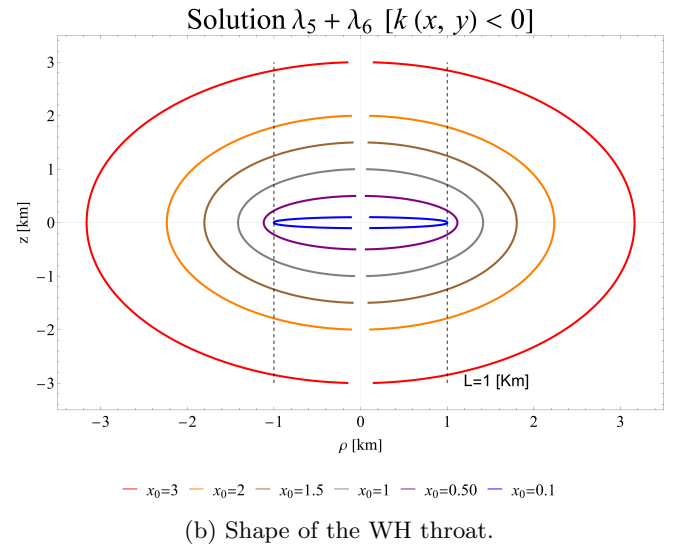
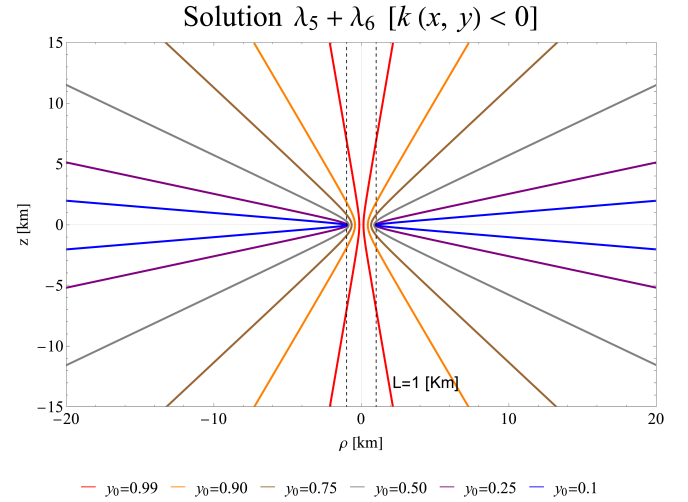


FIG. 1: The parameters $\lambda_0 = 10^{-2}$, $\tau_0 = 10^{-3}$, $k_0 = 1/12$, and a WH the size of the Sun have been used for both graphs. The initial condition used for the numerical solution is $z(x = 0)$. Furthermore, all units in the graphs are expressed in kilometers.

Hipersurface of $\lambda_5 + \lambda_6$ [$k(x, y) < 0$]

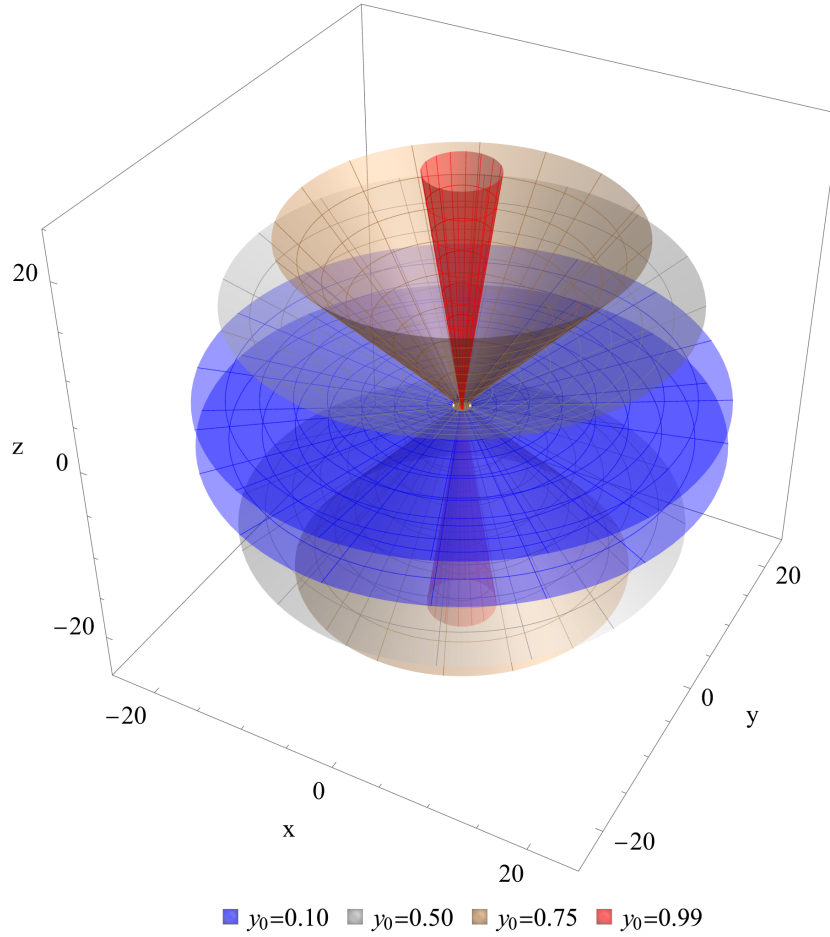


FIG. 2: Hypersurface characterizing the WH profile. It is constructed as a surface of revolution derived from the curves illustrated in [1a].

reference frame, we will consider his 4-velocity to be purely temporal $\vartheta^{\hat{\mu}} = (1, 0, 0, 0)$, which guarantees the orthogonality of the 4-acceleration and the 4-velocity $W^{\hat{\mu}}\vartheta_{\hat{\mu}} = 0$, which implies that $W^{\hat{\mu}} = (0, \hat{a}, 0, 0)$. Therefore, by using the geodesic deviation equation

$$\Delta a^{\hat{\mu}} = -c^2 R^{\hat{\mu}}{}_{\hat{\alpha}\hat{\beta}\hat{\sigma}} \vartheta^{\hat{\alpha}} \xi^{\hat{\beta}} \vartheta^{\hat{\sigma}}, \quad (42)$$

It is possible to determine the danger zones where the astronaut can be destroyed by tidal forces. Here $\xi^{\hat{\mu}}$ is the 4-distance between the astronaut's head and feet, and $R^{\hat{\mu}}{}_{\hat{\alpha}\hat{\beta}\hat{\sigma}}$ are the components of the Riemann tensor in the astronaut's reference frame. The Riemann tensor in $\hat{\mathbb{O}}$ is derived using the linear transformation matrix used in special relativity, which facilitates the transformation[24]

from \mathbb{O} to $\hat{\mathbb{O}}$.

$$\mathbb{M}_{RE} = \begin{bmatrix} \beta & -\gamma\beta & 0 & 0 \\ -\gamma\beta & \beta & 0 & 0 \\ 0 & 0 & 1 & 0 \\ 0 & 0 & 0 & 1 \end{bmatrix}, \quad (43)$$

where $\beta = \vartheta/c$, ϑ is the speed of $\hat{\mathbb{O}}$ with respect of \mathbb{O} , and $\gamma = 1/\sqrt{1 - \beta^2}$.

The relations of the Riemann components tensors are

$$R_{\hat{1}\hat{0}\hat{1}\hat{0}} = R_{1010}, \quad (44a)$$

$$R_{\hat{2}\hat{0}\hat{2}\hat{0}} = \gamma^2 R_{2020} + \gamma^2 \beta^2 R_{2121}, \quad (44b)$$

$$R_{\hat{3}\hat{0}\hat{3}\hat{0}} = \gamma^2 R_{3030} + \gamma^2 \beta^2 R_{3131}. \quad (44c)$$

Let $|\xi| \approx 2m$ be the astronaut's height and we consider that the maximum gravity that the human body can withstand is that of the Earth g_{Earth} , from which the following inequality is derived

$$|R_{\hat{\mu}\hat{0}\hat{\mu}\hat{0}}| \leq \frac{g_{Earth}}{2m * c^2} \approx (10^5 \text{Km})^{-2}. \quad (45)$$

If the astronaut travels at non-relativistic speeds. ($\beta \approx 0$ this implies that $\gamma \approx 1$), then $R_{\hat{\mu}\hat{0}\hat{\mu}\hat{0}} \approx R_{\mu_0\mu_0}$. Otherwise, it is necessary to consider the terms $R_{\mu_1\mu_1}$.

The Riemann components of the solution (24) in $\bar{\mathbb{O}}$ are

$$R_{1010} = \frac{(1-y^2)e^{-2k_c}}{4L^2(x^2+y^2)^5} \left(\lambda_0(y^2-x^2) + 2xy\tau_0 \right)^2, \quad (46a)$$

$$R_{2020} = \frac{e^{-2k_c}}{4L^2(x^2+y^2)^5} \left(\tau_0(x^2-y^2) + 2xy\lambda_0 \right)^2, \quad (46b)$$

$$R_{3030} = \frac{e^{-2k_c}}{4L^2(x^2+y^2)^4} \lambda_0^2 \left\{ 4xy(x^2-y^2) + \lambda_0^2(y^2(1-y^2) + x^2(3y^2+1)) + \tau_0^2(x^2(1+x^2-3y^2) + y^2) \right\}, \quad (46c)$$

$$R_{2121} = 4k_0 R_{3030}, \quad (46d)$$

$$R_{3131} = \frac{e^{-2k_c}}{4L^2(x^2+y^2)^5} \left\{ \lambda_0\tau_0 \left(16k_0x^5y + 4(8k_0-3)x^3y(1-y^2) + 4xy^3(4k_0(y^2-2) - 3y^2+3) \right) + \lambda_0^2 \left(x^4(y^2(20k_0-3) - 4k_0+3) - 2x^2y^2(4k_0(y^2-3) - 3y^2+3) + (4k_0-3)y^4(y^2-1) \right) + \tau_0^2 \left(4k_0x^4(1+x^2-2y^2) - 4x^2y^2(y^2(3-5k_0) + 6k_0-3) + 4k_0y^4 \right) \right\}. \quad (46e)$$

To graph tidal forces, we restrict our consideration to a spacecraft exhibiting non-relativistic velocities, thus employing only the equations (46a) - (46c) in (44). For this

purpose, we use the Boyer-Lindquist coordinates (r, θ) and a *Sun-sized wormhole*, whose parameters are determined by

$$M = M_\odot \approx 2 \times 10^{30} \text{Kg}, \quad (47a)$$

$$L < 2l_1 = R_s^{Sun} \approx 3 \times 10^3 \text{m}. \quad (47b)$$

In Figure 3, all components of non-relativistic tidal forces are represented. The left panel presents a 3D graph, while the right panel displays contour lines for better visualization of dimensions. Upon focussing on Fig. 3a, it becomes clear that a possible value across the WH is close to or ideally at the poles. However, Fig. 3c and Fig. 3e indicates that this statement is erroneous due to the presence of a barrier-like structure. All barrier-like structures in Fig. 3 are centered at $l_1 = R_s/2$, while all other areas show negligible tidal forces. The contour line of R_{2020} and R_{3030} reveals that the magnitude is finite (10^{-6}Km^{-2}) in regions near the poles but greater than the possible safe tidal force. To improve clarity we take the approximation $y \rightarrow 0$ within the equation (46):

$$R_{1010}(x, 1) = 0, \quad (48a)$$

$$R_{2020}(x, 1) = \frac{(2\lambda_0x + \tau_0(x^2-1))^2}{4L^2(x^2+1)^4}, \quad (48b)$$

$$R_{3030}(x, 1) = R_{2020}(x, 1), \quad (48c)$$

In this way we can observe that all the components remain finite in the vicinity of the poles.

In equations (46) and (48), it is clear that the parameter L plays an important role. This is because an increase of 10 in L leads to a significant decrease in tidal forces by a factor of 10^{-2} . After this reduction, by assigning $L = 10^3 \text{Km}$, so that $L < l_1 = 1.5 \times 10^3 \text{Km} = R_s^{WH}/2$, each element of the tidal forces resides within a safe domain for traversing the massive WH ($M_{WH} = 10^3 M_\odot$), since its dimensions are less than $\approx 10^{-10} \text{Km}^{-2}$. The safe regions are then $\theta \in [0, 3\pi/16] \cup (13\pi/16, \pi]$.

If we restrict ourselves to a WH corresponding to these solutions and which has parameters indicative of a safe and stable size, it could exhibit the following characteristics

$$L \geq 10^3 \text{Km} \quad \text{which implies that} \quad M_{WH} \geq 10^3 M_\odot. \quad (49)$$

VIII. GEODESICS

A. Lagrangian and Hamiltonian formulation

The Lagrangian and Hamiltonian formulations are crucial for studying particle dynamics. Using the metric, we

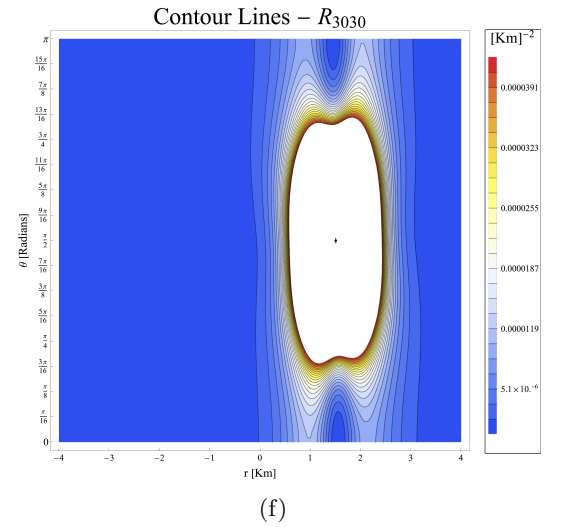
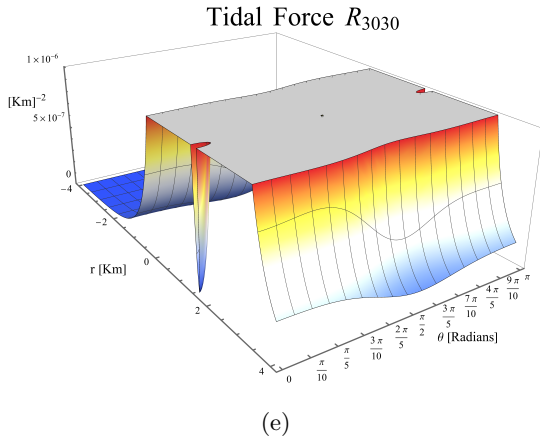
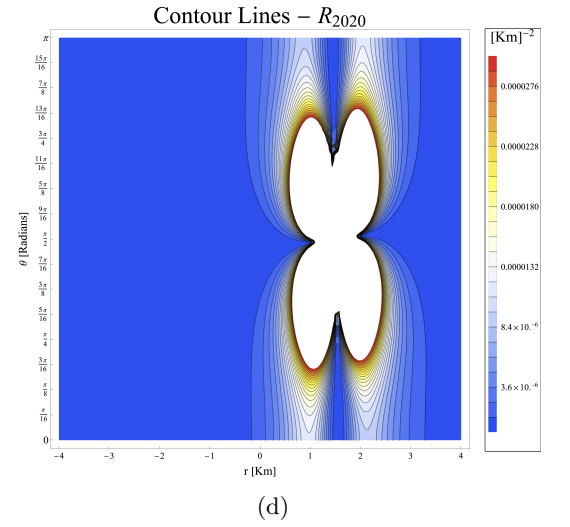
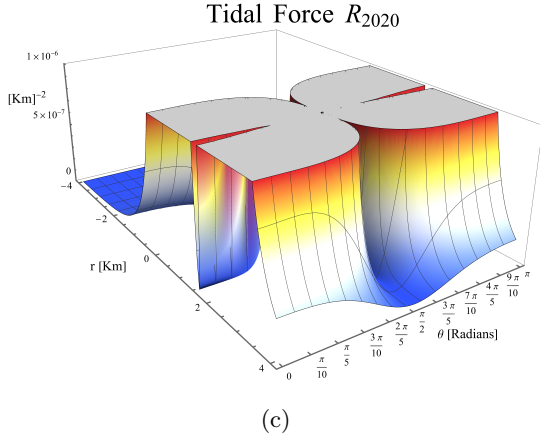
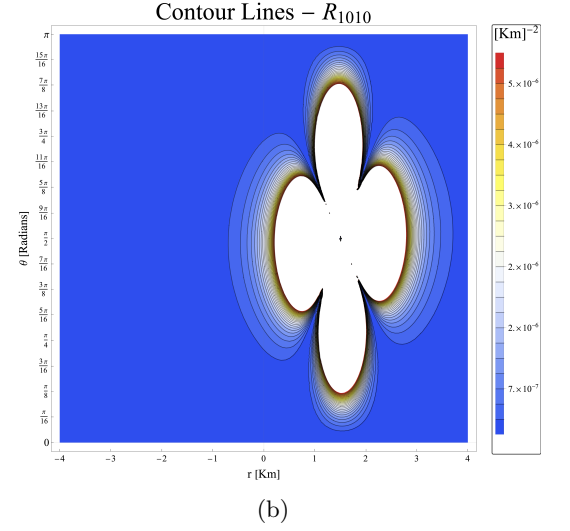
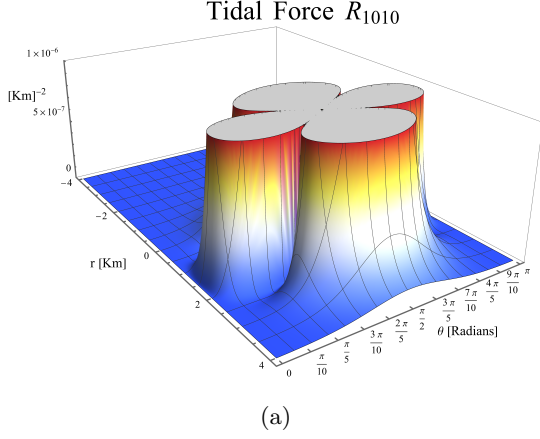


FIG. 3: Tidal forces at non-relativistic velocities, all plots use the parameters $\lambda_0 = 10^{-2}$, $\tau_0 = 10^{-3}$, $k_0 = 1/12$ and values for a celestial object of the mass of the Sun. The images on the left represent three-dimensional plots; the horizontal plane represents a plane described by the coordinates (r, θ) , while the vertical axis defines the magnitude of each component of the tidal force $R_{\mu_0\mu_0}$ expressed in Km^{-2} .

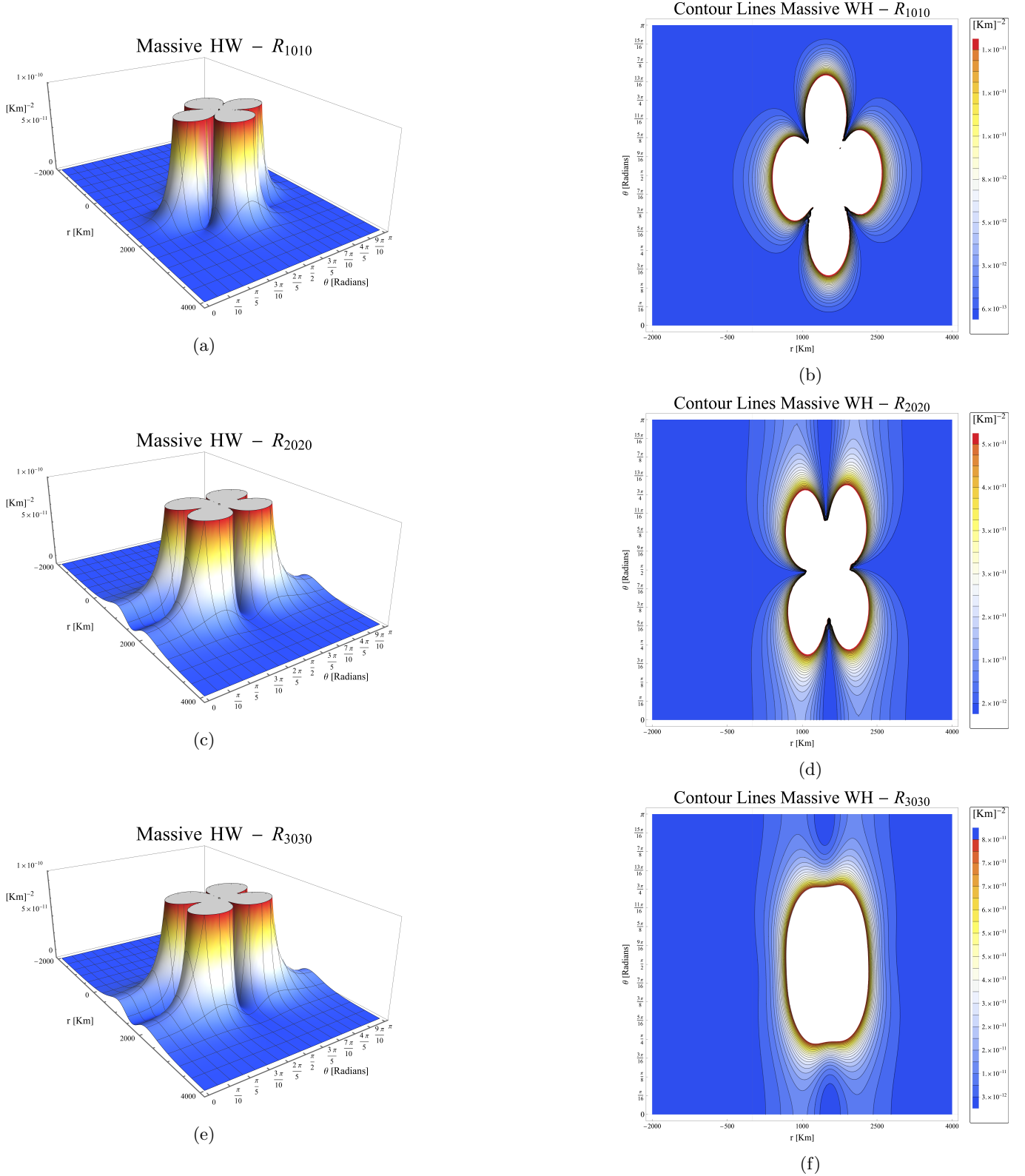


FIG. 4: Tidal forces are considered at non-relativistic velocities with parameters identical to those in Figure 3, except for the parameters $l_1 = 1.5 \times 10^3 \text{Km}$ which implies $L = 10^3 \text{Km}$, where they are scaled by a factor of 10^3 times the Schwarzschild radius of the Sun. Three-dimensional plots are constrained by an upper bound of 10^{-10}Km^{-2} , on the magnitude axis.

can derive the corresponding Lagrangian $2\mathcal{L} \equiv g_{\mu\nu}\dot{x}^\mu\dot{x}^\nu$, so we have

$$2\mathcal{L} = -f(ct - \omega\dot{\varphi})^2 \frac{L^2}{f} \left\{ (x^2 + 1)(1 - y^2)\dot{\varphi}^2 + e^{2k}(x^2 + y^2) \left(\frac{\dot{x}^2}{x^2 + 1} + \frac{\dot{y}^2}{1 - y^2} \right) \right\}, \quad (50)$$

where $\dot{t} \equiv dt/ds$, and s is an affine parameter.

From (50), we can derive the moments using $p_\mu \equiv \partial\mathcal{L}/\partial x^\mu$. There are two cyclic coordinates (t, φ) , therefore the constants of motion (E, l_z) are

$$-p_t = E = f(ct - \omega\dot{\varphi}), \quad (51a)$$

$$p_\varphi = l_z = \frac{L^2(x^2 + 1)(1 - y^2)}{f}\dot{\varphi} + \omega E. \quad (51b)$$

Isolating \dot{t} and $\dot{\varphi}$ from the equations (51), we can divide the two to derive the angular velocity

$$\frac{\dot{\varphi}}{\dot{t}} = \frac{d\varphi}{dt} = \frac{f^2(l_z - \omega E)c}{L^2(x^2 + 1)(1 - y^2)E + f^2\omega(l_z - \omega E)}, \quad (52)$$

The other two moments are determined by

$$p_x = \frac{L^2(x^2 + y^2)e^{2k}}{f(x^2 + 1)}\dot{x}, \quad (53a)$$

$$p_y = \frac{L^2(x^2 + y^2)e^{2k}}{f(1 - y^2)}\dot{y}. \quad (53b)$$

To obtain the Hamiltonian, it is necessary to evaluate $2\mathcal{H} \equiv g^{\mu\nu}p_\mu p_\nu$. Considering all momentum components and the inverse metric (10), the corresponding Hamiltonian can be determined as

$$2\mathcal{H} = \frac{f(l_z - \omega E)^2}{L^2(x^2 + 1)(1 - y^2)} - \frac{E^2}{f} + \frac{f e^{-2k}}{L^2(x^2 + y^2)} \left\{ (x^2 + 1)p_x^2 + (1 - y^2)p_y^2 \right\}. \quad (54)$$

From the expressions for the moment, we obtain the moment norm, which is given by

$$g^{\mu\nu}p_\mu p_\nu = (mass_0)^2 c^2 = 2\mathcal{H},$$

where $(mass_0)$ represents the rest mass, that is, for photons we have $(mass_0) = 0$. Therefore, to determine the initial conditions corresponding to the null geodesics, it is necessary to impose the condition $\mathcal{H}(x^\mu, p^\mu) = 0$ to (54).

Taking advantage of the metric functions (24), the initial condition is derived, taking the values

$$l_z = 1, \quad E = 2, \quad (55a)$$

$$x(0) = 25, \quad p_x(0) = -2, \quad p_y(0) = 0, \quad (55b)$$

and arbitrary $y(0) = y_0$.

B. Null geodesic graphics

The equations of motion are derived from Hamilton's equations given by

$$\dot{x}^\mu \equiv \frac{\partial\mathcal{H}}{\partial p_\mu}, \quad (56a)$$

$$\dot{p}_\mu \equiv -\frac{\partial\mathcal{H}}{\partial x^\mu}. \quad (56b)$$

Now using the initial condition (55), which defines the null geodesics, and the resulting equation of motion (56), we can obtain a numerical solution that allows us to construct a plot of x against y to examine the behavior of the null geodesic as it passes through the WH or fails to encounter the causally disconnected singularity. In Figure 5a, the null geodesics corresponding to different initial conditions y_0 are represented by various colors. The graphics employ spheroidal coordinates to enhance the visualization of the ring singularity, represented by a gray dot. The reference $x > 0$ denotes one universe, while $x < 0$ indicates a different universe or the same universe in another region. It is observed that the geodesic identified as $y_0 = 0.95$, particularly those near the poles, cannot pass through the WH. In contrast, all other null geodesics pass through the WH unimpeded.

Figures 5d, 5c, and 5b illustrate the trajectory of the photons in a representation in Cartesian coordinates in the cylindrical coordinates

$$X_c = \rho \cos\left(\frac{d\varphi}{dt}t\right),$$

$$Y_c = \rho \sin\left(\frac{d\varphi}{dt}t\right),$$

$$Z_c = z.$$

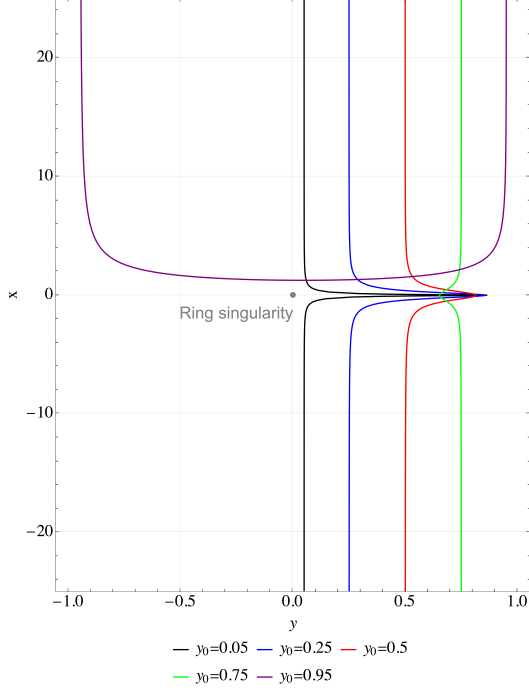
The ring singularity is represented as a blue circle with a radius specified as L . The gray curves in each graph indicate one universe, while the orange curves represent the scenario in which the particle passes through the WH into another universe. For clarity, different colors are used to represent this transition.

When a photon travels toward the singularity through the equatorial plane ($y_0 = 0$), it takes an infinite time to reach it, indicating that the ring singularity is causally disconnected. This behavior is illustrated in Figure 6. Note that the coordinate $x(s)$ never intersects the axis $x^\mu(s) = 0$, while the coordinate $y(s)$ reaches that axis in a short period of time, but subsequently maintains a constant trajectory. $y(s) \neq 0$.

To contact the singularity, the coordinate functions $x(s)$, $y(s)$ of the null geodesic must simultaneously coincide with the axis $x^\mu(s) = 0$.

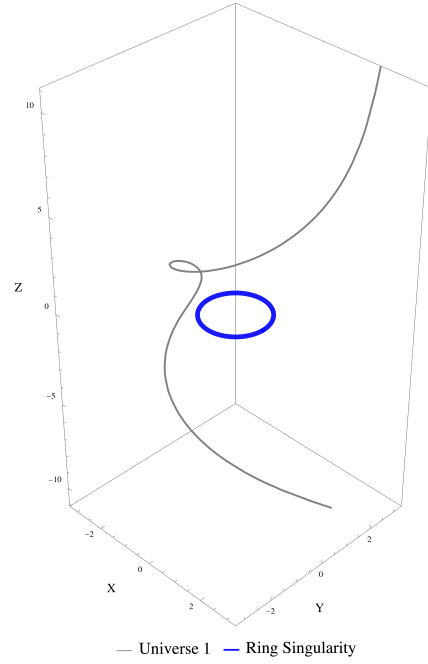
To determine the duration of the path of a null geodesic, we start from the Lagrangian (50) expressed in cylindrical coordinates (ρ, z) . We incorporate the equa-

Null geodesics in spheroidal coordinates $\lambda_5+\lambda_6$



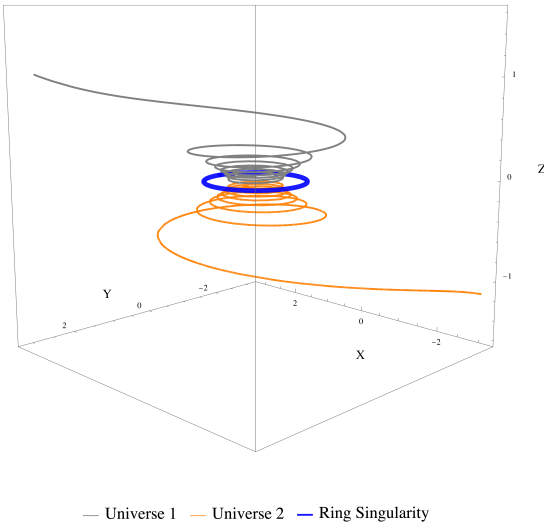
(a) Null geodesics for different values of y_0 in (x, y) -coordinates. Positive values of x correspond to one universe, while negative values of x pertain to either another universe or the same universe in a distinct spatial region.

Null geodesic of $\lambda_5+\lambda_6$ ($\theta_0=18.20^\circ$)



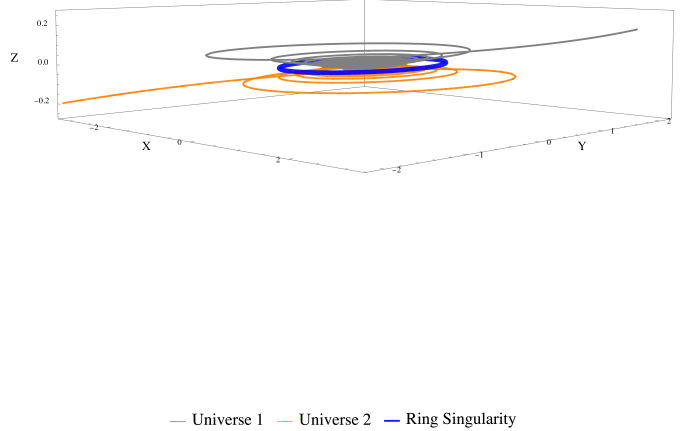
(b) A null geodesic path commencing at a polar angle $\theta_0 = 18.20^\circ$ which does not pass through the WH.

Null geodesic of $\lambda_5+\lambda_6$ ($\theta_0=75.52^\circ$)



(c) A null geodesic path starting at a polar angle $\theta_0 = 75.52^\circ$ passing through the WH.

Null geodesic of $\lambda_5+\lambda_6$ ($\theta_0=87.13^\circ$)



(d) A null geodesic path starting at a polar angle $\theta_0 = 87.13^\circ$ passing through the WH.

FIG. 5: Null geodesic curves that satisfies (55) and with parameters $\lambda_0 = 10^{-2}$, $\tau_0 = 10^{-3}$, $k_0 = 1/12$, and Sun size WH.

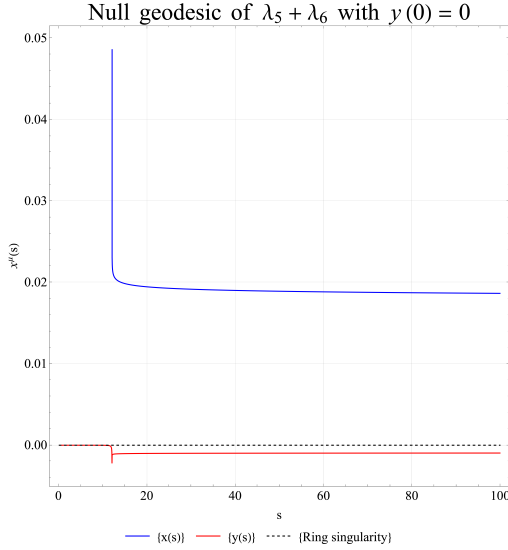


FIG. 6: Null geodesic coordinates that satisfies (55) and with parameters $y_0 = 0$, $\lambda_0 = 10^{-2}$, $\tau_0 = 10^{-3}$, $k_0 = 1/12$, and Sun size WH, directed to the ring singularity.

tions (5) and the initial conditions (55) in (50), to obtain

$$2\mathcal{L} = \frac{e^{2k}}{f}(\dot{\rho}^2 + \dot{z}^2) - \frac{1}{f} \left(E^2 - \frac{f^2(l_z - \omega E)^2}{\rho^2} \right), \quad (57)$$

So, if we set $2\mathcal{L} = 0$, we get the equations of motion for the photons, and we can see the shape of the effective potential

$$\begin{aligned} (\dot{\rho}^2 + \dot{z}^2) &= \frac{e^{-2k}}{f} \left(E^2 - \frac{f^2(l_z - \omega E)^2}{\rho^2} \right) \\ &\equiv \bar{E} - V_{eff}. \end{aligned} \quad (58)$$

However, if we define $\dot{\Delta}^2 \equiv (\dot{\rho}^2 + \dot{z}^2)$ this implies that $d\Delta_{|y:cte}^2 \equiv (d\rho^2 + dz^2)_{|y:cte}$ represents the line element associated with the two-dimensional subspace generated by ρ, z for a y_0 value, we can integrate the equality (58) with $y = y_0$. The resulting integral is

$$s = \int_{x_0}^{x_1} \frac{e^{k(x, y_0)} d\Delta_{|y:cte}}{\sqrt{E^2 - f^2(l_z - \omega(x, y_0)E)^2 / \rho(x, y_0)^2}} \quad (59)$$

where

$$d\Delta_{|y:cte} = \sqrt{(d\rho^2 + dz^2)_{|y:cte}} = L \sqrt{\frac{x^2 + y_0^2}{x^2 + 1}} dx.$$

If we keep a fixed coordinate, for example $x_0 = 1$ in (59), and we graph the function $-s(x_1)$ considering $x_1 \rightarrow 0$

and incorporating the parameters given in (55a), it can be observed in Figure 7 that the time required for the null geodesic to hit the ring singularity tends to infinity as we approach zero. This is again shown by numerical

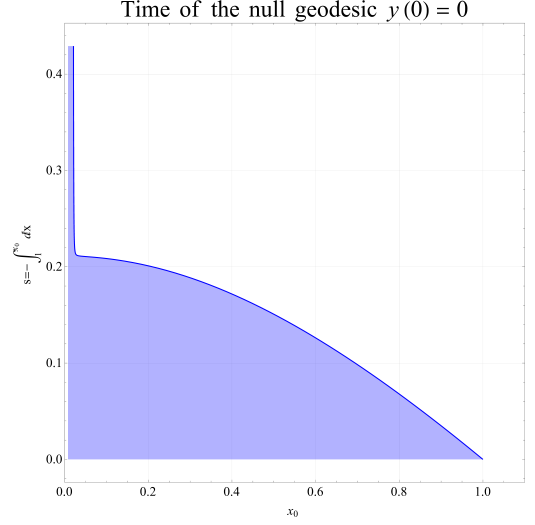


FIG. 7: Value of the integral (59) using $\lambda_0 = 10^{-3}$, $\tau_0 = 10^{-2}$ and a WH the size of the Sun.

integration that the ring singularity is causally disconnected.

The effective potential of the photons associated with this WH, as derived in (58), is then

$$V_{eff} \equiv \frac{f^2(l_z - \omega E)^2}{\rho^2} e^{-2k}, \quad (60)$$

and its minimal unstable points are identified by

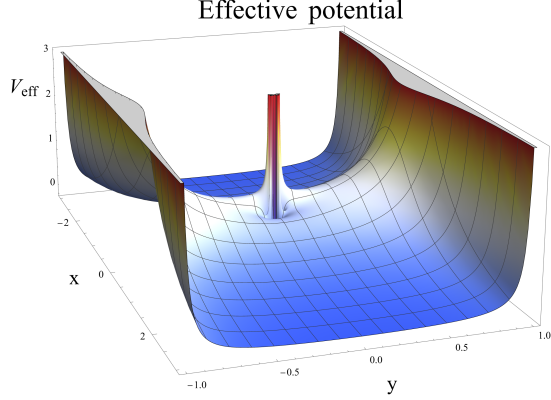
$$\begin{aligned} \frac{d}{dx} V_{eff} &= 0, \\ \frac{d^2}{dx^2} V_{eff} &< 0. \end{aligned}$$

Figure 8 shows the effective potential profile. In Fig.8a, the complete three-dimensional effective potential is represented by spheroidal coordinates. Figure 8b provides a more detailed view of the effective potential profile near the equatorial plane. It is evident that near the equatorial plane, the effective potential is asymmetric, indicating that antisymmetry arises naturally in this type of WH.

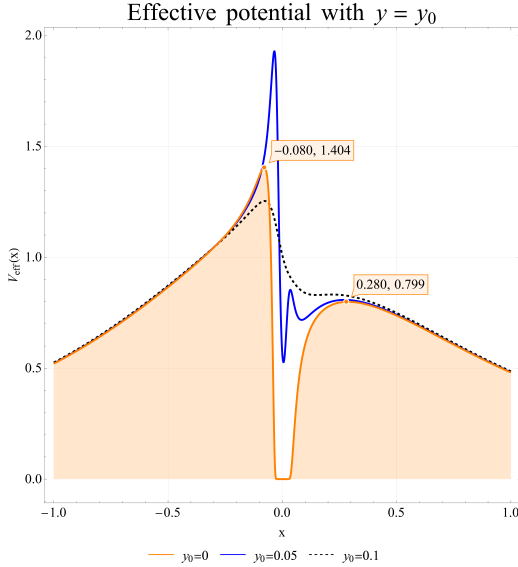
To derive the corresponding dimensions of the parameters, we have employed equations (7), (8), (24), (55a), (52), $\lambda_0 = 10^{-2}$, $\tau_0 = 10^{-3}$ together with the formulation of the electromagnetic field described by

$$\begin{bmatrix} B_z \\ -B_\rho \end{bmatrix} = \frac{-1/\sqrt{\sigma_0}}{L(x^2+y^2)} \frac{\sqrt{f_0}}{2\kappa_0} \begin{bmatrix} x\sqrt{(x^2+1)(1-y^2)} & -y\sqrt{(x^2+1)(1-y^2)} \\ y(x^2+1) & x(1-y^2) \end{bmatrix} \begin{bmatrix} \partial_x \\ \partial_y \end{bmatrix} \left(\frac{\omega}{L} e^{-\lambda} \right), \quad (61a)$$

$$\begin{bmatrix} E_\rho \\ E_z \end{bmatrix} = \frac{c/\sqrt{\sigma_0}}{L(x^2+y^2)} \frac{\sqrt{f_0}}{2\kappa_0} \begin{bmatrix} x\sqrt{(x^2+1)(1-y^2)} & -y\sqrt{(x^2+1)(1-y^2)} \\ y(x^2+1) & x(1-y^2) \end{bmatrix} \begin{bmatrix} \partial_x \\ \partial_y \end{bmatrix} (e^{-\lambda}), \quad (61b)$$



(a) Effective potential in 3 dimensions.

(b) Effective potential with a constant $y = y_0$.

The orange curve $y_0 = 0$ represents the equatorial plane and its non-nestable equilibrium points.

FIG. 8: The parameters used are $\lambda_0 = 10^{-2}$, $\tau_0 = 10^{-3}$, $k_0 = 1/12$, $L = 1$, and (55a) in the equation (60).

In these equations, E represents the electric field and B the magnetic field, measured in volts per meter and tesla, respectively. Assuming the WH has an oblate spheroidal geometry where the polar radius R_p is one-third the size of the equatorial radius R_e , the formula for angular mo-

mentum is [25]

$$J = \frac{10}{45} M r^2 \frac{d\varphi}{dt}. \quad (62)$$

The angular velocity and consequently the electromagnetic field, along with all related parameters, can be calculated by setting $\theta = \pi/4$ and considering a meditation radii $r = \{7 \times 10^8, 10^5, 10^{12}\}$ m that correspond to the

positions at which the desired physical quantity is to be measured [26]. Table II shows the parameters associated with a Sun-sized WH $M = M_\odot$, a magnetar-sized WH $M = 2M_\odot$, and a supermassive WH $M = 10^7 M_\odot$.

IX. ELECTROMAGNETIC FIELD

To visualize the detailed electromagnetic field in (61), we use the metric functions described in (24). This allows us to observe a schematic representation of the fields. For this graph, the parameters are set as $\lambda_0 = 10^{-2}$, $\tau_0 = 10^{-3}$ and $c = 1$, $\sigma_0 = 1$, $L = 1$, $l_1 = 1.5$.

In what follows, we will obtain corresponding graphs within a singular Cartesian frame, for this, we will propose Cartesian coordinates whose transformation with Boyer-Lindquist coordinates is given by

$$\begin{aligned} Lx + l_1 = r &= \sqrt{u^2 + v^2 + w^2}, \\ y = \cos \theta &= w/r, \end{aligned}$$

where (u, v, w) denote the Cartesian coordinates and $|r| \geq l_1$. Substituting this relation into (61), it is possible to decompose the components of the electromagnetic field by

$$\begin{aligned} H_u(u, v, w) &= H_\rho(u, v, w) \cos\left(\frac{d\varphi}{dt}t\right), \\ H_v(u, v, w) &= H_\rho(u, v, w) \sin\left(\frac{d\varphi}{dt}t\right), \\ H_w(u, v, w) &= H_z(u, v, w), \end{aligned}$$

where $H = B, E$, and $d\varphi/dt = \frac{d\varphi}{dt}(u, v, w)$.

There are several important observations to make. First, the equatorial plane $y = 0$ corresponds to the plane $w = 0$, indicating that the ring singularity lies at the points $w = 0$ and $l_1^2 = u^2 + v^2$. Secondly, it is crucial to note that the internal values of the sphere with radius $x = 0 \Rightarrow r = l_1$ determined by $r < l_1$, are forbidden, which indicates that this region does not constitute a part of space-time. Consequently, there are two critical regions in the electromagnetic field within these coordinates. Figure 9 illustrates the vector fields corresponding to the magnetic and electric fields, shown in the first and second rows, respectively.

In the Figure 9, the ring singularity has been represented by a torus. It is important to note that all graphs are schematic representations and do not represent actual values in SI units. The key point is that, in the regions adjacent to the ring singularity, the electromagnetic field is remarkably strong, and at the ring singularity itself, the electromagnetic field diverges, tending toward infinity. The ring singularity lies within the forbidden inner region, which corresponds to the sphere with radius $r = l_1$.

Despite the considerable intensity found near the ring singularity, navigation through the WH remains possible. Along the polar axis, there is a possible opening.

To facilitate a more thorough analysis, it is necessary to analytically examine the asymptotic behavior of the electromagnetic field, taking into account its dependencies (r, θ) .

$$B_\rho(r, \pi/2) = \frac{e^{L\tau_0/(r-l_1)}}{(r-l_1)^4 \sqrt{\sigma_0}} \left(-\lambda_0^2 L^3 + \tau_0(r-l_1)(L^2 + (r-l_1)^2) \right), \quad (63a)$$

$$B_z(r, \pi/2) = -\frac{e^{L\tau_0/(r-l_1)}}{(r-l_1)^4 \sqrt{\sigma_0}} \sqrt{1 + \frac{(r-l_1)^2}{L^2}} \lambda_0 \left(L\tau_0 + l_1 - r \right), \quad (63b)$$

$$E_\rho(r, \pi/2) = -\frac{e^{L\tau_0/(r-l_1)} L^2 \tau_0 c}{(r-l_1)^3 \sqrt{\sigma_0}} \sqrt{1 + \frac{(r-l_1)^2}{L^2}}, \quad (63c)$$

$$E_z(r, \pi/2) = -\frac{e^{L\tau_0/(r-l_1)} L^2 \tau_0 c}{(r-l_1)^3 \sqrt{\sigma_0}}, \quad (63d)$$

$$B_\rho(r, 0) = -\frac{e^{-L(L\lambda_0 - \tau_0(r-l_1)) / (L^2 + (r-l_1)^2)}}{(L^2 + (r-l_1)^2)^2 \sqrt{\sigma_0}} L\tau_0 \left(\tau_0(L^2 - (r-l_1)^2) - 2L\lambda_0(r-l_1) \right), \quad (64a)$$

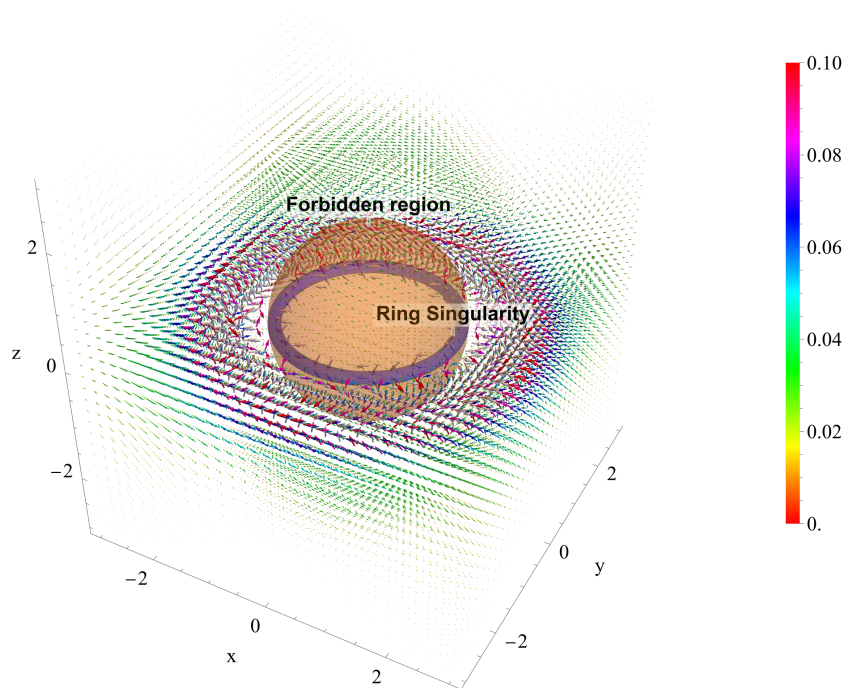
$$B_z(r, 0) = 0, \quad (64b)$$

$$E_z(r, 0) = -\frac{e^{-L(L\lambda_0 - \tau_0(r-l_1)) / (L^2 + (r-l_1)^2)}}{(L^2 + (r-l_1)^2)^2 \sqrt{\sigma_0}} c L \left(\tau_0(L^2 - (r-l_1)^2) - 2L\lambda_0(r-l_1) \right), \quad (64c)$$

$$E_\rho(r, 0) = 0, \quad (64d)$$

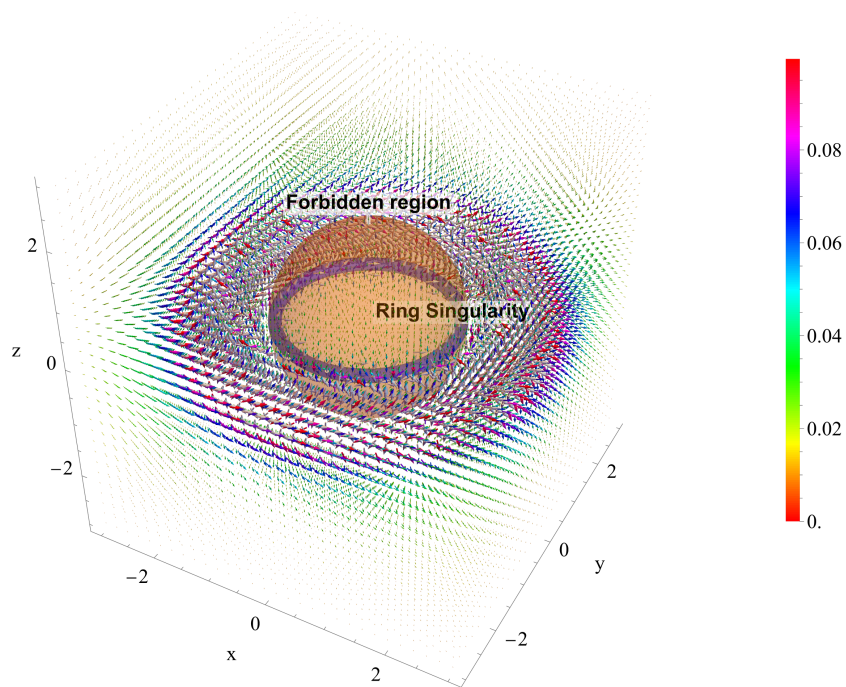
Here it is convenient to separate the two critical regions, starting with the equatorial plane, as described in the equations (63). Graphing these equations, we obtain figures 10a and 10c. The regions close to the ring singularity present notably high values. These graphical representations and equations (63) illustrate that, in both scenarios, the field diverges at the ring singularity, designated as the points $r = l_1$ and $\theta = \pi/2$. In all other regions, the electromagnetic field maintains finite values. If we now consider the equations presented in (64), we can generate Figures 9a and 9b, which clearly show that

Magnetic Field



(a)

Electric Field



(b)

FIG. 9: Diagrammatic electromagnetic vector field.

TABLE II: Description of the WH parameters. The first row, listing three different values of L , is associated with a WH comparable to a Sun-like structure, described by a Sun-sized black hole. Here, a radius almost equal to that of the Sun is assumed, approximately $r \approx 7 \times 10^8$ m. The second row presents three values of L representative of a magnetar-like WH, characterized by $M = 2M_\odot$, $R_s \approx 6 \times 10^3$ m, and a radius of approximately $r \approx 10^5$ m. Finally, the third row, which also presents three values of L , corresponds to a WH similar to a supermassive black hole, defined by $M = 10^7 M_\odot$, $R_s \approx 3 \times 10^{10}$ m, and a radius around $r \approx 10^{12}$ m.

L (Meters)	$d\varphi/dt$ (Seconds ⁻¹)	a (Meters)	$Q_L^2 + H_L^2$ (Meters)	E (Volt/Meters)	B (Teslas)
10^1	6.205×10^{-10}	2.254×10^{-1}	2.181×10^6	1.064×10^7	-1.757×10^6
10^2	6.984×10^{-10}	2.537×10^{-1}	2.191×10^6	1.064×10^8	-1.757×10^6
10^3	1.477×10^{-9}	5.365×10^{-1}	3.181×10^6	1.064×10^9	-1.757×10^6
10^1	3.228×10^{-2}	2.393×10^{-1}	8.722×10^6	5.549×10^{14}	-1.270×10^{10}
10^2	3.630×10^{-2}	2.691×10^{-1}	8.732×10^6	5.658×10^{15}	-1.295×10^{10}
10^3	7.356×10^{-2}	0.545×10^{-1}	9.722×10^6	6.746×10^{16}	-1.544×10^{10}
10^1	3.132×10^{-16}	2.322×10^{-1}	2.181×10^{20}	5.372×10^0	-1.248×10^3
10^3	7.456×10^{-16}	5.527×10^{-1}	2.181×10^{20}	5.372×10^2	-1.248×10^3
10^5	4.398×10^{-14}	3.261×10^1	2.181×10^{20}	5.372×10^4	-1.248×10^3

when crossing the WH at either pole, the electromagnetic field remains finite. However, in this type of WH ($M = M_\odot$), the intensity of the electromagnetic field that an astronaut would have to endure is such as to make the crossing unfeasible. However, based on the equations presented in (64), it becomes evident that the value depends on L . For example, when considering a WH with mass $M = 10^7 M_\odot$, the maximum values of the magnetic field along the polar axis are approximately 1700 Teslas.

X. CONCLUSIONS

The novel combined solution λ_c exhibits properties very similar to those observed in [18] and [19], albeit with minor differences. It is noteworthy that the ring singularity is preserved in the spatial characteristic, and the Null Energy Condition (NEC) is satisfied by appropriately selecting a dilatonic scalar field. Analyzing the WH geometry, it is evident that the profile and shape of its throat vary with respect to the polar entry angle. When traversing the WH within the equatorial plane, the minimum value of the throat approaches L and its shape tends to close. Similarly, the the WH throat encloses ring singularity. When examining the possibility of traversing the WH along the polar axis, no impediments to traversal were observed.

Summarizing the findings from the analyses of tidal forces, electromagnetic fields, and geodesics, a compelling proposal can be articulated. The optimal entry angle, without encountering impediments, lies along the polar axis, or perhaps close to it. This is attributed to the fact that, along this axis, both tidal forces and electromagnetic fields are minimal and finite. To traverse the WH, the initial energy required exceeds the maximum thresholds of the effective asymmetric barrier potential. To establish a minimum limit for assessing the safety of a WH size, it is clear that considering tidal forces suggests that the optimal dimensions correspond to a massive WH with a mass $M \geq 10^3 M_\odot$. However, incorporating the effects of the electromagnetic field, the safest dimensions for a WH would be $M \geq 10^7 M_\odot$, analogous to a supermassive WH located at the center of the Milky Way.

This work contains several significant elements. A

barrier-like structure of tidal forces is centered around the ring singularity (figures 3 and 4), which represents an obstacle to any life form attempting to approach the singularity due to the spaghettification phenomenon. However, within the ring singularity itself, these tidal forces are absent. An intense electromagnetic field is present near the ring singularity (figures 9), which causes the polarization and subsequent destruction of physical bodies. This is a critical barrier that prevents contact with the ring singularity. Specifically, the electromagnetic field at the ring singularity is considered infinite. Furthermore, the inner region $r < l_1$ is forbidden.

Another significant aspect presented in this article is the inherent asymmetry of the proposed WH's effective potential (figure 8). This feature is crucial, as it allows WHs to be observed and distinguished from black holes based on their shadow, as discussed in [27], [28].

The ring singularity is causally disconnected, as directing a photon toward this singularity requires an infinite time to reach it from the equatorial plane. This statement is corroborated by numerical solutions. For an analytical analysis of the non-causal contact of the singular ring, one can see [22]

However, the most interesting consequence of the present work is that if the dilatonic interaction exists, that is, if there are phenomena where the scalar field is the source of the electromagnetic field of a celestial body, then the existence of traversable celestial WHs is possible. In fact, any theory that predicts extra dimensions, such as superstring theory [29], Kaluza-Klein theories [30],[31], [32] or Brans-Dicke theory [33], contains a dilaton field with exactly the interaction proposed here in Lagrangian (1). In other words, the main result of the present work is that theories such as superstring theory, Kaluza-Klein or Brans-Dicke theory predict the existence of realistic celestial WHs, or the existence of celestial WHs in nature.

XI. ACKNOWLEDGEMENTS

LB thanks SECIHTI-México for the doctoral grant. This work was also partially supported by SECIHTI México under grants A1-S-8742, 304001, 376127, 240512.

-
- [1] A. Einstein, The foundation of the general theory of relativity., *Annalen Phys.* **49**, 769 (1916).
 - [2] A. Einstein, Approximative Integration of the Field Equations of Gravitation, *Sitzungsber. Preuss. Akad. Wiss. Berlin (Math. Phys.)* **1916**, 688 (1916).
 - [3] B. P. Abbott *et al.* (LIGO Scientific, Virgo), Observation of Gravitational Waves from a Binary Black Hole Merger, *Phys. Rev. Lett.* **116**, 061102 (2016), arXiv:1602.03837 [gr-qc].
 - [4] K. Schwarzschild, On the gravitational field of a mass point according to Einstein's theory, *Sitzungsber. Preuss. Akad. Wiss. Berlin (Math. Phys.)* **1916**, 189 (1916), arXiv:physics/9905030.
 - [5] J. R. Oppenheimer and H. Snyder, On Continued gravitational contraction, *Phys. Rev.* **56**, 455 (1939).
 - [6] K. Akiyama *et al.* (Event Horizon Telescope), First M87 Event Horizon Telescope Results. I. The Shadow of the Supermassive Black Hole, *Astrophys. J. Lett.* **875**, L1 (2019), arXiv:1906.11238 [astro-ph.GA].
 - [7] A. Einstein, Cosmological Considerations in the General Theory of Relativity, *Sitzungsber. Preuss. Akad. Wiss. Berlin (Math. Phys.)* **1917**, 142 (1917).

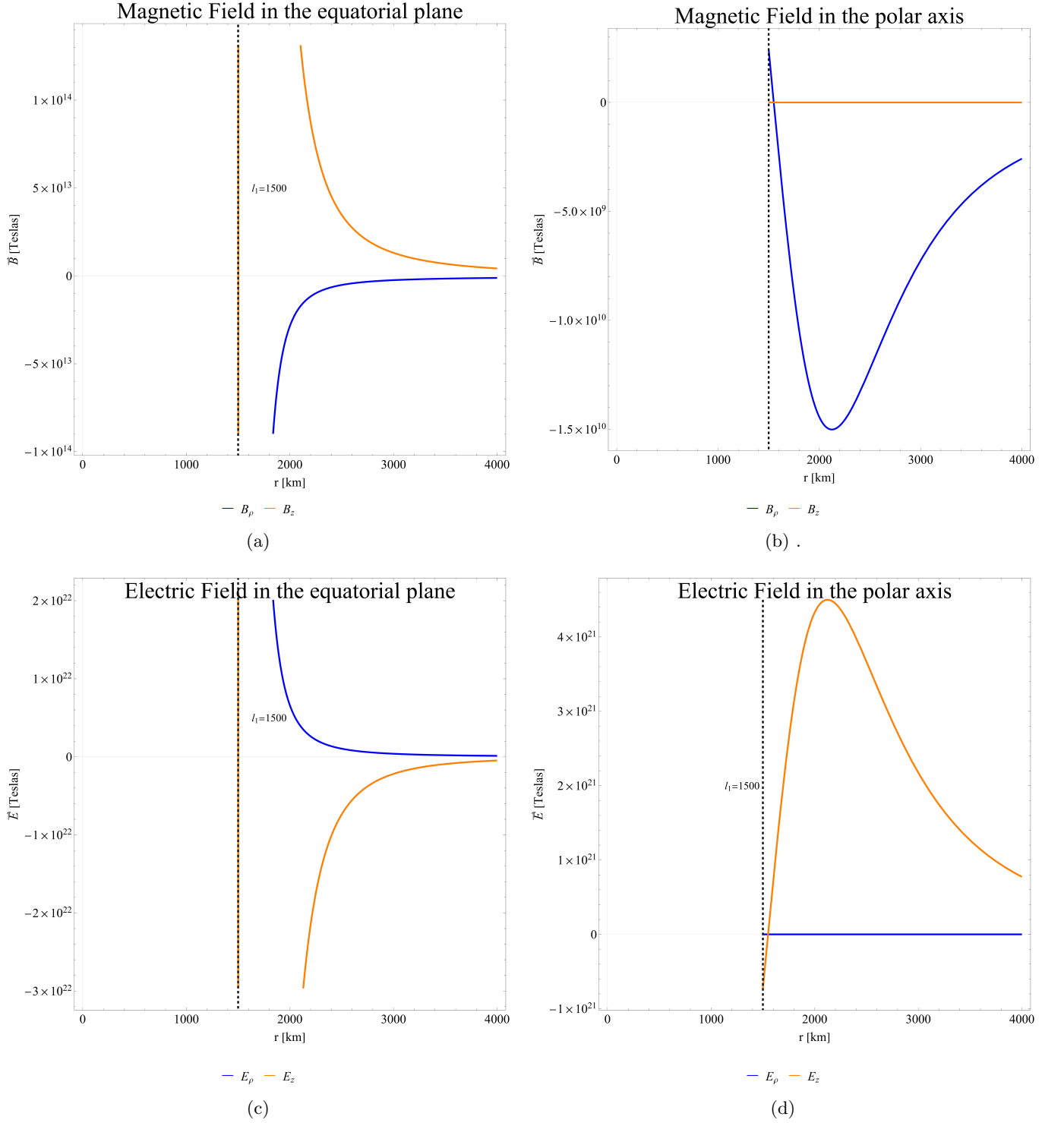


FIG. 10: This figure illustrates the electromagnetic fields in the equatorial plane, as shown in the left column with the reference $y = 0$, and along the polar axis, as shown in the right column with the reference $y = \pm 1$. These graphs represent a WH with a mass $M = M_{\odot}$.

- [8] E. Hubble, A relation between distance and radial velocity among extra-galactic nebulae, *Proc. Nat. Acad. Sci.* **15**, 168 (1929).
- [9] A. G. Riess *et al.* (Supernova Search Team), Observational evidence from supernovae for an accelerating universe and a cosmological constant, *Astron. J.* **116**, 1009 (1998), arXiv:astro-ph/9805201.
- [10] A. Einstein and N. Rosen, The Particle Problem in the General Theory of Relativity, *Phys. Rev.* **48**, 73 (1935).
- [11] T. Matos, Class of Einstein-Maxwell Phantom Fields: Rotating and Magnetised Wormholes, *Gen. Rel. Grav.* **42**, 1969 (2010), arXiv:0902.4439 [gr-qc].
- [12] T. Matos, L. A. Urena-Lopez, and G. Miranda, Wormhole Cosmic Censorship, *Gen. Rel. Grav.* **48**, 61 (2016), arXiv:1203.4801 [gr-qc].
- [13] J. C. Del Águila and T. Matos, Wormhole Cosmic Censorship: An Analytical Proof, *Class. Quant. Grav.* **36**, 015018 (2019), arXiv:1806.03747 [gr-qc].
- [14] T. Matos, D. Nunez, G. Estevez, and M. Rios, Rotating 5-D Kaluza-Klein space-times from invariant transformations, *Gen. Rel. Grav.* **32**, 1499 (2000), arXiv:gr-qc/0001039.
- [15] T. Matos, D. Nunez, and M. Rios, Class of Einstein-Maxwell dilatons, an ansatz for new families of rotating solutions, *Class. Quant. Grav.* **17**, 3917 (2000), arXiv:gr-qc/0008068.
- [16] T. Matos and D. Nunez, Rotating scalar field wormhole, *Class. Quant. Grav.* **23**, 4485 (2006), arXiv:gr-qc/0508117.
- [17] T. Matos, G. Miranda, R. Sanchez-Sanchez, and P. Wiederhold, Class of Einstein-Maxwell-Dilaton-Axion Space-Times, *Phys. Rev. D* **79**, 124016 (2009), arXiv:0905.4097 [gr-qc].
- [18] J. C. Del Águila, T. Matos, and G. Miranda, Exact Rotating Magnetic Traversable Wormholes satisfying the Energy Conditions, *Phys. Rev. D* **99**, 124045 (2019), arXiv:1507.02348 [gr-qc].
- [19] L. Bixano and T. Matos, Einstein-Maxwell-dilaton wormholes that meet the energy conditions, *Phys. Rev. D* **111**, 084056 (2025), arXiv:2502.07206 [gr-qc].
- [20] The differential equation for k arises from the integration of one of the components of the field equation 4c.
- [21] F. S. N. Lobo, ed., *Wormholes, Warp Drives and Energy Conditions*, *Fundamental Theories of Physics*, Vol. 189 (Springer, 2017) arXiv:2103.05610 [gr-qc].
- [22] J. C. Del Águila and T. Matos, Geodesic completeness of a ring wormhole, *Phys. Rev. D* **107**, 064047 (2023), arXiv:2303.12251 [gr-qc].
- [23] M. S. Morris and K. S. Thorne, Wormholes in space-time and their use for interstellar travel: A tool for teaching general relativity, *Am. J. Phys.* **56**, 395 (1988).
- [24] The transformation matrix (43) only transforms the covariant components.
- [25] Following the methodology outlined in [19], we derive the parameters in a comparable manner.
- [26] In Boyer-Linquist coordinates (r, θ) .
- [27] M. Wielgus, J. Horak, F. Vincent, and M. Abramowicz, Reflection-asymmetric wormholes and their double shadows, *Phys. Rev. D* **102**, 084044 (2020), arXiv:2008.10130 [gr-qc].
- [28] F. H. Vincent, M. Wielgus, M. A. Abramowicz, E. Gourgoulhon, J. P. Lasota, T. Paumard, and G. Perrin, Geometric modeling of M87* as a Kerr black hole or a non-Kerr compact object, *Astron. Astrophys.* **646**, A37 (2021), arXiv:2002.09226 [gr-qc].
- [29] M. B. Green and J. H. Schwarz, Anomaly Cancellation in Supersymmetric D=10 Gauge Theory and Superstring Theory, *Phys. Lett. B* **149**, 117 (1984).
- [30] D. Wuensch, *Kaluza—klein theory* (Springer Berlin Heidelberg, 2009) pp. 328–331.
- [31] T. Kaluza, Zum Unitätsproblem der Physik, *Sitzungsber. Preuss. Akad. Wiss. Berlin (Math. Phys.)* **1921**, 966 (1921), arXiv:1803.08616 [physics.hist-ph].
- [32] O. Klein, Quantum Theory and Five-Dimensional Theory of Relativity. (In German and English), *Z. Phys.* **37**, 895 (1926).
- [33] C. Brans and R. H. Dicke, Mach's principle and a relativistic theory of gravitation, *Phys. Rev.* **124**, 925 (1961).